An International Journal of Optimization and Control: Theories & Applications
ISSN: 2146-0957 eISSN: 2146-5703
Vol.16, No.1, pp.138-159 (2026)
https://doi.org/10.36922/IJOCTA025340146

RESEARCH ARTICLE

A methodology for calculating the load-bearing capacity of pile foundations in offshore hydraulic structures based on principles of rational design

Latif F. Aslanov[1,2†*] and Ulvi L. Aslanli[3,4†]

[1]Department of Hydrotechnical Construction, Laboratory of Study of Marine Hydraulic Structures, Oil Gas Scientific Research Project Institute, Baku, Azerbaijan
[2]Department of Engineering Communication Systems, Faculty of Water Management, Construction and Land Reclamation, Azerbaijan University of Architecture and Construction, Baku, Azerbaijan
[3]Department of Industrial Enterprises Design, Oil Gas Scientific Research Project Institute, Baku, Azerbaijan
[4]Department of Foundations, Bases and Underground Structures, Azerbaijan University of Architecture and Construction, Baku, Azerbaijan
Latif.Aslanov@socar.az, ulvi.l.aslanli@socar.az

ARTICLE INFO

Article History:
Received: August 23, 2025
Revised: October 4, 2025
Accepted: October 23, 2025
Published Online: November 22, 2025

Keywords:
Drilled-in piles
Load-bearing capacity
Offshore engineering
Pile foundations
Soil–structure interaction

AMS Classification 2010:
90B23, 90B56

ABSTRACT

The bearing capacity of piles in soil is determined by both the mechanical properties of the soil and the method of pile installation. The widespread implementation of pile foundations in offshore oil and gas field development has highlighted significant deficiencies in the current domestic scientific, methodological, and regulatory approaches for evaluating pile–soil interaction. This study addresses the key issues and limitations in calculating bearing capacity for commonly used drilled-in and precast piles. For combined drilled-in piles, the existing methodology inaccurately assumes that the hydrostatic pressure exerted by the cement slurry on the borehole walls remains unchanged after hardening, leading to erroneous estimations. In the case of precast metal piles, the use of standardized regulatory tables results in substantial discrepancies compared to actual performance, particularly at depths exceeding 35 m, where these methods become completely inapplicable. Furthermore, the dynamic method outlined in building regulations—used to predict the bearing capacity of short precast piles driven using mechanical or hydraulic hammers in offshore environments—produces results with unacceptable margins of error. This method is also unsuitable for longer piles due to its inherent limitations. The root causes of the limitations in existing methods for evaluating the load-bearing capacity of pile foundations have been systematically investigated. Based on this analysis, the theoretical framework for a new calculation methodology has been developed. By integrating comprehensive laboratory data, a revised approach is proposed that significantly enhances the reliability and accuracy of the estimated bearing capacity, ensuring closer alignment with actual field performance. The bearing capacity and settlement of pile foundations for offshore hydraulic structures were computed and analyzed with consideration of the soil's plastic deformation behavior.

1. Introduction

The fixation of hydrotechnical facilities for oil and gas extraction to seabed soils within the Caspian Sea region is predominantly achieved through pile foundation systems. Ensuring the structural strength and stability of these hydraulic constructions during both the design and construction

†*These authors contributed equally to this work.*
*Corresponding Author

phases necessitates addressing numerous theoretical and practical challenges. To this end, extensive static and dynamic experimental investigations have been conducted both *in situ* within the Caspian Sea and under controlled laboratory conditions to provide solutions and enhance the reliability of foundation design.

Recent studies have extensively addressed various aspects related to the load-bearing capacity of pile foundations. Alekseev and Bezvolev [1] investigated the determination of maximum pile capacity based on the torsional moment developed during pile installation. Similarly, Alzabeebee et al. [2] proposed a novel model for evaluating pile bearing capacity, while Angurana et al. [3] examined the influence of factors, such as embedment depth, friction angle, screw blade to shaft diameter ratio, spiral count, and spacing on the performance of screw piles using finite element analysis.

Innovative methodologies have also been introduced to enhance prediction accuracy. An intelligent system was developed employing an adaptive neuro-fuzzy inference framework optimized via the imperialist competition algorithm to forecast pile load-bearing capacity. [4] Extensive investigations have contributed substantially to understanding the stress–strain behavior of offshore hydraulic structures under varied permanent and transient loading conditions. [5–15]

To address soil heterogeneity in standard settlement calculations, an elastic layer foundation model akin to an elastic half-space was proposed by Ref. [16], while laboratory tests were conducted on sand bases reinforced with jute geotextiles. [17] Elastoplastic analyses of shallow rigid foundations were also performed, considering Winkler-type soil behavior and elastic compliance via model correction factors. [18]

Advanced modeling techniques have been applied in related structural analyses, such as the use of finite element models based on higher-order shear deformation theories to analyze buckling in porous functionally graded sandwich plates on elastic Winkler-Pasternak foundations. [19] Improvements to machine learning-based prediction models have been achieved by integrating optimization algorithms. [20] A comprehensive model simulating cylindrical foundations under torsional vibrations has been developed, [21] while bearing capacity for various foundation types, including pile groups and slabs, has been evaluated using experimental data and finite element tools. [22]

Field validation efforts include pile testing studies, [23] and an integral estimation method was introduced for settlement prediction of homogeneous foundations. [24] Collectively, these works underscore the multifaceted approaches being developed to improve the reliability and precision of pile foundation design in complex geotechnical environments.

Recent research has focused on various aspects of pile foundation behavior under different soil and loading conditions. The load transfer mechanisms at both the pile body and the tip for multiple pile-group configurations in saturated and unsaturated soils with varying properties were investigated. [25] Field experiments examined the performance of full-scale pile foundations installed in sand, loess, and composite soil layers under diverse loading scenarios. [26] Additional investigations into load distribution and deformation characteristics in stratified soils were also presented. [27] A numerical method was developed to analyze bridge abutment pile foundations affected by karst-induced deformations, accounting for negative skin friction along the pile shaft. [28]

In geotechnical characterization studies, site zones were defined based on mechanical parameters, including seismic activity, depth, wave velocity, Young's modulus, shear modulus, and Poisson's ratio, for highly compacted soil layers. [29] Settlement behavior, bearing capacity, axial forces, and skin friction responses were evaluated for both permeable and impermeable concrete piles. [30] The load-bearing capacity of concrete piles embedded in clayey and sandy soils was modeled and compared with that of polyurethane piles. [31]

Additional investigations include finite element analysis of failure zones around octagonal foundations under undrained conditions at zero interface stress, [32] comparative assessments of bottom-lifting piles in layered soils, [33] and a comprehensive review of static, dynamic, and numerical methods for predicting axial pile capacity, including field load tests. [34] The influence of inhomogeneous elastic foundations on the free vibration of composite plates reinforced with functional-grade graphene in fluid environments was explored, [35] while pile end behavior in layered liquefied and non-liquefied soils was studied. [36]

Collectively, these studies advance understanding of pile foundation performance in complex geotechnical settings, highlighting the necessity for integrated experimental, numerical, and analytical approaches.

Recent advancements in pile foundation research have focused on both experimental and computational approaches to better understand pile behavior under complex loading conditions. Static and combined load tests on a practical model comprising 16 piles arranged into eight

groups were conducted to assess the bearing capacity of piles in sandy soils subjected to multidirectional loads. [37] Methodologies for determining the soil deformation modulus based on punch test results were proposed, contributing to improved subsurface characterization. [38]

Further developments include studies on micropile-raft design and associated installation techniques (Kong et al. [39]), and the analysis of vertical compressive load effects on molded piles. [40] Kumar et al. [41] compared multiple deep learning algorithms—such as deep neural networks, convolutional neural networks, recurrent neural networks, long short-term memory, and bidirectional models—using dynamic pile-loading datasets to evaluate their predictive performance.

Axisymmetric finite element solutions were developed for assessing the bearing capacity of ring foundations resting on anisotropic and heterogeneous clays, [42] while the most reliable interpretation technique for cast-in-place pile testing was identified. [43] A three-dimensional (3D) numerical analysis explored the lateral response of underexpanded piles in clay, [44] and pile-loading tests were performed to quantify surface friction and end-bearing resistance in both soil and rock conditions. [45]

Analytical modeling efforts were furthered by applying a three-variable higher-order shear deformation theory to analyze the dynamic behavior and stability of functionally graded beams on variable elastic foundations. [46] Stress distributions near pile shafts and toes were investigated through 3D simulations in the presence of tunnel-induced ground movement. [47,48] Load transfer mechanisms in socketed piles embedded in synthetic soft rock were examined using miniature pile test rigs. [49]

Additionally, the sequential impact of basement excavation and tunneling on single-pile response was studied. [50] An efficient hybrid machine learning model integrating genetic algorithms with artificial neural networks was introduced for the rapid prediction of pile capacity. [51] A method for calculating equivalent elastic constants in complex environments based on classical elasticity theory and the principle of superposition was presented. [52]

These contributions collectively underscore the diversity of modern pile foundation research, ranging from machine learning and advanced numerical modeling to experimental field investigations and analytical solutions.

Recent developments in geotechnical engineering have increasingly incorporated artificial intelligence and advanced modeling techniques to enhance the prediction and analysis of foundation behavior. Deep neural networks have been employed to estimate the axial load capacity of piles, [53], while ground settlement variations have been assessed using Sentinel-1 satellite imagery and the Sentinel Application Platform software, highlighting the growing role of remote sensing in geotechnical monitoring. [54] A model has been proposed to predict the settlement of single bored piles by accounting for the elastoplastic response of soils, [55] and the effectiveness of machine learning techniques in forecasting pile bearing capacity has also been demonstrated. [56]

In addition, PLAXIS-2D was utilized to generate a parametric dataset for simulating the settlement of shallow foundations above circular cavities. [57] Principal characteristics and input parameters of three commonly used soil constitutive models were examined, [58] while the deformation behavior of rock masses subjected to strip foundation pressure was investigated. [59] Nonlinear vibration responses of inhomogeneous anisotropic shallow shell structures resting on elastic foundations defined by Pasternak's two-parameter model were studied. [60]

Further contributions include the application of feedback neural networks to model geotechnical behavior [61] and field investigations involving four static load tests on grooved piles across different construction sites. [62] Horizontal load tests on rectangular piles before and after concrete casting were performed to evaluate structural integrity. Li et al. [63] The seismic response of reinforced concrete buildings in relation to foundation settlement and soil typology was addressed. [64]

The non-uniform distribution of compressive modulus gradients in soil particles and the stiffness of soil skeletons across depth profiles in unsaturated road subgrades were analyzed. [65] In a subsequent study, the effect of these gradients on the dynamic response of subgrades under uniform traffic loading was examined. [66] A two-hybrid model—combining radial basis function and multilayer perceptron neural networks—optimized using an arithmetic optimization algorithm, was utilized to estimate the load-bearing capacity of driven piles based on experimental data. [67]

These studies collectively underscore the growing integration of data-driven models, numerical simulations, and field validation in improving the accuracy and efficiency of foundation performance assessment in complex soil environments.

Recent research has increasingly focused on advanced modeling techniques and data-driven

approaches to improve the understanding of foundation behavior in heterogeneous and complex geotechnical conditions. The application of tree-based machine learning algorithms to estimate the axial load capacity of piles was explored, providing an efficient alternative to conventional predictive models. [68] The influence of spatial variability in soil properties on the bearing capacity of rigid foundations under conditions involving large deformations was examined, emphasizing the need for probabilistic approaches in foundation analysis. [69]

A uniform carbonate distribution model was proposed to investigate the mechanical response of biocemented soils, employing the discrete element method to simulate the heterogeneous nature of biocemented samples and enhance the understanding of microstructural behavior. [70] A concrete–rock shear interaction model based on statistical characterization of the random fragmentation of rock was developed, offering a more realistic representation of shear mechanisms in mixed materials. [71]

The Gaussian distribution law was referred to model greenfield conditions, and the equivalent beam method was adopted to account for both bending and shear deformations in structures. The analysis incorporated residual soil deformation and the potential separation between buildings and the underlying ground, leading to a detailed investigation of the interrelationships between building settlement, structural load, and the number of stories. [72]

Collectively, these studies highlight the integration of statistical, numerical, and machine learning techniques as vital tools for enhancing the predictive capabilities of geotechnical models, particularly in scenarios involving material heterogeneity and complex soil–structure interactions.

In the construction of offshore structures in shallow zones of the Caspian Sea, the use of relatively short piles (10–15 m in length) during preliminary installation stages is typically assessed using Gersevanov's dynamic formula, which provides sufficiently accurate estimations under these conditions. However, for longer piles, the application of this method leads to significant discrepancies—ranging from 1.5 to 2.0 times deviation—when compared to actual measured load-bearing capacities, thereby limiting its reliability in deepwater or complex scenarios.

Despite these limitations, the control of the designed driving depth for piles installed using mechanical or drop hammers continues to rely on this approach. In practice, pile driving is considered complete once a penetration refusal criterion—typically defined as less than 15 mm of settlement over 10 consecutive hammer blows—is achieved, based on calculations derived from this method.

The dynamic method plays a crucial role in evaluating the stress–strain behavior of the hammer–pile system during installation, as well as in identifying and mitigating potential overloads and structural failures resulting from impact forces. To address the limitations of conventional approaches, a novel dynamic prediction methodology is developed to account for the propagation of impact waves within the system during the pile-driving process. This approach is particularly suited for controlling hammer–pile interactions in varying driving conditions and for predicting the load-bearing capacity of large-diameter piles used in deepwater offshore environments.

2. Materials and methods

The bearing capacity and settlement of pile foundations for offshore hydraulic structures were analyzed using a comprehensive engineering approach that incorporated the nonlinear behavior of soil, including plastic deformation. The pile was modeled as a one-dimensional elastic bar subjected to dynamic hammer impacts, governed by wave propagation equations.

To realistically simulate soil–pile interaction, Koiter's associated flow rule was employed to describe plastic strain increments, with yield surfaces estimated using segmented linear functions. A nonlinear soil resistance model incorporating viscous, elastic, and plastic components was used to characterize the soil response.

Numerical modeling was performed using the finite element method (FEM) to capture the complex behavior of the pile and surrounding soil. This enabled detailed simulation of stress distribution, deformation, and nonlinear material behavior under dynamic loading.

Structural and geotechnical analyses in this study were performed using Structural Analysis Computer System (SACS 5.5 8Vi, Bentley Systems, USA) and Structural Analysis and Design Professional (STAAD Pro V8i, Bentley Systems, USA), enabling the modeling of pile dynamics, structural response, and verification of compliance with design standards. The selection of these software tools was based on their system requirements, computational efficiency, and widespread adoption in engineering practice, ensuring that the methodology remains practically applicable and accessible to engineers. In addition, laboratory data on soil mechanical properties were

integrated to calibrate and validate the numerical models, providing reliable results aligned with field observations. The proposed approach complies with relevant local and international standards, including American Petroleum Institute Recommended Practice 2A and International Organization for Standardization 19901, making it suitable for offshore structural engineering applications.

3. Results

3.1. Model development and numerical methodology

From a theoretical standpoint, the method is grounded in a one-dimensional dynamic analysis of force wave propagation within the hammer–pile–soil system. This analysis is performed using numerical techniques, specifically the FEM, which enables precise simulation of wave behavior and interaction across system components. By modeling the pile as a one-dimensional elastic bar, the general behavior of wave propagation induced by hammer impacts can be accurately described and utilized to optimize driving efficiency and ensure structural safety Equation (1).

$$\frac{\partial^2 u}{\partial t^2} = F(u, x, t) \tag{1}$$

Let $u = u_{(x,t)}$ denote the displacement of a pile cross-section at position x and time t, where u is expressed in m and t in s. The governing equation includes an integro-differential operator F, which characterizes the internal stress response of the pile cross-section while accounting for the viscous, elastic, and plastic resistance of the surrounding soil medium.

Due to the analytical challenges associated with modeling the complex physical and mechanical behavior of the soil, the hammer–pile–soil interaction system is simplified by representing it as a discrete system composed of individual elements with defined constitutive behaviors-namely elastic, plastic, and viscous characteristics (Figure 1). This abstraction allows for the replacement of the original governing integro-differential equation with a set of computationally manageable relationships.

As a result, the complex system of equations governing pile dynamics is reduced to a series of sequentially solvable expressions, enabling step-by-step numerical evaluation of the displacement and stress distribution within the pile elements during the driving process Equation (2).

$$u_{i,t} = u_{i,t-1} + \Delta t \nu_{i,t-1} \tag{2}$$

The elastic interaction forces between adjacent pile elements are defined by Equation (3).

$$F_{i,t} = k_i \left(u_{i,t} - u_{i-1,t}\right) \tag{3}$$

where $F_{i,t}$ represents the elastic force at time t between the i-th and $(i-1)$-th pile segments, k_i is the stiffness coefficient of the corresponding segment, and $u_{i,t}$ and $u_{i-1,t}$ denote the displacements of the respective elements.

For the modeling of plastic deformations, additional constitutive relationships are incorporated to account for the irreversible displacement behavior of pile elements once the yield limit is exceeded. These formulations enable a more accurate representation of the pile's response under high-impact dynamic loading conditions Equations (4)–(6).

$$U^0_{i,t} = \begin{cases} u_{i,t} + Q_i \ for \ u_{i,t} + Q_i < u^0_{i,t-1}, \\ u^0_{i,t-1} \ for \ u_{i,t} + Q_i \geq u^0_{i,t-1} - Q_i \ , \\ u^0_{i,t} - Q_i \ for \ u^0_{i,t} - Q_i > u^0_{i,t-1}, \end{cases} \tag{4}$$

$$v_{i,t} = v_{i,t-1} + \left(F_{i-1,t} - F_{i,t} - R_{i,t}\right) \frac{\Delta t}{m_i} \tag{5}$$

for the velocities of the elements

$$\begin{aligned} &R_{i,t} = \left(u_{i,t} - u^0_{i,t}\right) \cdot P_i \cdot \{1 + (\tau_i \nu_{i,t-1})^{\mu} \\ &sign\left[\left(u_i - u^0_i\right) \nu_t\right] \end{aligned} \tag{6}$$

for the resistance of soil to elements.

The key variables used in the dynamic analysis of the hammer–pile–soil system are defined as follows:

- $u_{i,t}$: total displacement of the i-th pile element at time t, measured in meters (m);
- $u^0_{i,t}$: plastic (irreversible) component of displacement of the i-th pile element at time t, in minutes;
- $v_{i,t}$: velocity of the i-th element at time t, in meters per second (m/s);
- $F_{i,t}$: internal force acting on the i-th pile element at time t, in kilonewtons (kN);
- k_i: longitudinal stiffness (axial rigidity) of the i-th element, expressed in kilonewtons per centimeter (kN/cm);
- m_i: mass of the i-th pile element, in metric tons (t);
- Δt: time interval for the propagation of the stress (impact) wave through the element, in seconds (s); this value is selected based on the wave transmission characteristics of the material.

This formulation enables a time-discrete representation of the dynamic process and forms the

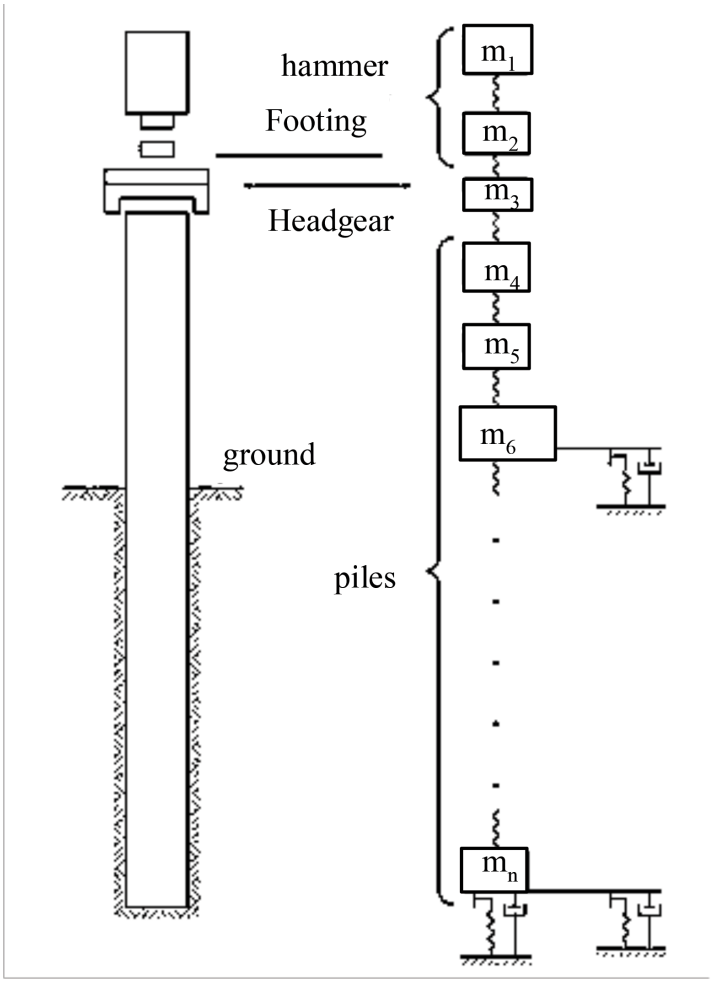

Figure 1. The scheme of partition of the pile into finite elements

basis for numerical simulation using the FEM Equation (7).

$$\Delta t \leq \min \left(\frac{m_i}{x_i} \right)^{\frac{1}{2}} \tag{7}$$

Let Q_i represent the elastic deformation limit of the soil interacting with the i-th pile element. For most soil types, this value typically ranges from 0.1 to 0.4 cm.

The term $R_{i,t}$ denotes the resistance exerted by the soil on the i-th pile element at time t, measured in kilonewtons (kN). The parameter P_i defines the external frictional stiffness of the soil acting on the pile within the elastic deformation range, expressed in kilonewtons per centimeter (kN/cm).

The coefficient τ_i is the soil viscosity factor. For lateral (shaft) resistance, its value generally ranges between 0.001 and 0.004 s/cm, while for axial (tip) resistance, it typically falls within the range of 0.005–0.01 s/cm. It is important to note that the values of both τ and Q_i are selected with consideration of the soil's density within the specified intervals. As soil density increases (or in the case of clays, as water content decreases), these parameters also tend to increase accordingly. The symbol μ denotes the viscosity index of the soil, which commonly varies within the interval of 0.3–0.5.

The initial dynamic state of the system at the moment of impact is defined by a set of initial conditions that initiate the numerical simulation process.

$$u_{i,0} = u^0_{i,0} = 0, \; F_{i,0} = 0$$

where $\nu_{i,0} = 0$ for the pile's head and pile elements; and $\nu_{i,0} = \nu$ for the impact part of the hammer.

Naturally, several key parameters in the theoretical framework of the proposed method must be defined based on the specific properties of various soil types. To this end, a series of specialized laboratory experiments and *in situ* tests were conducted to establish accurate input values.

In the mathematical modeling process for calculating the axial load-bearing capacity and settlement of a thin-walled tubular pile under vertical static loading, the interaction between the

pile and the soil foundation is considered within the framework of solid-body mechanics. The computational domain is treated as a piecewise-homogeneous medium consisting of various soil layers and the pile material. The interaction between the pile and the surrounding soil is modeled as a deformable heterogeneous continuum.

Since the piles are assumed to be bodies of revolution and the loads are applied axially, axial symmetry conditions are used. The resulting boundary value problem is expressed by the differential equations of plasticity theory. Within the pile, the stress–strain relationships are described using Hooke's law, while for the soil, nonlinear relations from plastic flow theory with hardening are applied. The adopted model employs Koiter's associated flow rule Equation (8).

$$d\varepsilon_{ij}^{p} = \sum_{r} d\lambda^{r} \frac{\partial f_{r}}{\partial \sigma_{ij}} \tag{8}$$

Here, ε_{ij}^{p} and σ_{ij} represent the components of the plastic strain tensor and the stress tensor, respectively. $d\lambda^{r} \geq 0$ are scalar parameters determined from the loading conditions. The loading surface equation f_r is described using three linear segments Equations (9)–(12).

$$f_{r=1} = \sigma_1 - \sigma_{okt}\left(\omega_1\right) + \sigma.tg\varphi_{okt}(\omega_1) \tag{9}$$

$$f_{r=2} = \sigma_1 - \left[P_{okt}^{*}\left(\omega_1, \omega_v\right) + \sigma\right] \cdot tg\psi_{okt}(\omega_1) \tag{10}$$

$$f_{r=3} = \sigma + P_{okt}\left(\omega_1, \omega_v\right) \tag{11}$$

where,

$$\begin{gathered} \sigma_{okt}\left(\omega_1\right) = \sigma_{okt}^{0} + \left(\sigma_{okt}^{*} - \sigma_{okt}^{0}\right) \cdot f\left(\frac{\omega_1}{\omega_1^{*}}\right) \\ \mathrm{tg}\varphi_{okt}\left(\omega_1\right) = \mathrm{tg}\varphi_{okt}^{0} + \left(\mathrm{tg}\varphi_{okt}^{*} - \mathrm{tg}\varphi_{okt}^{0}\right) \cdot f\left(\frac{\omega_1}{\omega_1^{*}}\right) \\ P_{okt}\left(\omega_1, \omega_v\right) = P_{okt} + \frac{\left(\left(P_{okt} \cdot tg\varphi_{okt}^{*} + \sigma_{okt}^{*}\right) \cdot f\left(\frac{\omega_1}{\omega_1^{*}}\right)\right)}{f\left(\frac{\omega_v}{\omega_v^{*}}\right)} \end{gathered} \tag{12}$$

Here, σ_{okt}^{0}, φ_{okt}^{0}, and ψ_{okt}^{0} are the parameters defining the position of the initial yield surface; σ and σ_1(the first and second invariants of the stress tensor).

To solve the system of nonlinear differential equations, the FEM in displacements is adopted. For this purpose, the considered domain is divided into toroidal (ring-shaped) elements, obtained by revolving triangular elements around the axis of symmetry. Displacements within each triangular element are estimated using first-order polynomials. Assuming the domain is divided into N elements, the governing equation of the problem can be written as Equation (13).

$$[k] \cdot \{u\} = \{F\} \tag{13}$$

where $[k] = \sum_{e=1}^{N} [k^e]$. Here, $[k^e]$, $[k]$ are the stiffness matrix of an individual finite element and the global stiffness matrix of the entire system, respectively, in the global coordinate system. $[F] = \sum_{e=1}^{N} [F^e]$ is the force vector, which includes all forces caused by external loads, initial stresses, initial strains, etc. u is the vector of unknown displacements.

Boundary conditions specified in the form of nodal displacements are taken into account by modifying the corresponding rows and columns of the stiffness matrix.

After assembling the stiffness matrix [k] and the force vector $\{F\}$, the vector of nodal displacements $\{u\}$ is determined by solving the system of algebraic equations Equation (5).

The solution of the system is significantly simplified by the fact that the stiffness matrix is symmetric and positive definite. Therefore, the Cholesky decomposition method (also known as the square root method) is applied to solve the equation system Equation (5).

The algorithm for solving the nonlinear problem is based on an iterative process that accounts for the development of plastic deformations. Since the components of the stress tensor are uniquely related to the elastic components of strain, the main objective of the algorithm is to decompose the total strain into elastic and plastic components.

Assuming that at time step $t-1$, the components of the displacement vector $\{u\}_{t-1}$, as well as the components of the total strain $\{\varepsilon\}_{t-1}$ and plastic strain $\left\{\varepsilon^{P}\right\}_{t-1}$, are known. The components of the displacement vector at time step t can then be obtained by solving the following system of equations Equations (14) and (15).

$$[k] \cdot \{u\}_t = \{F\} + \{F_{\varepsilon^p}\}_{t-1} \tag{14}$$

where the components of the vector $\{F_{\varepsilon^p}\}_{t-1}$ are obtained by integrating Equation (15).

$$\{F_{\varepsilon^p}\}_{t-1} = -\int_{v} [B]^{T} \cdot [D] \cdot \left\{\varepsilon^{P}\right\}_{t-1} dV \tag{15}$$

where $[B]^T$ is the differential operator of the static equilibrium equations, and $[D]$ is the elastic property matrix of the finite element. The global stiffness matrix remains constant throughout the computation process. In this case, the square root

method (Cholesky decomposition) leads to significant computational time savings, since the matrix $[k]$ can be decomposed into triangular form only once, and then only back-substitution is required to obtain new values of the primary unknowns.

The components of the total strain tensor at time step t are determined based on Cauchy's relations: $\{\varepsilon\}_t = [B] \cdot \{u\}_t$. At the first approximation, the position of the yield surface at time step t is assumed to be the same as at time step $t-1$, and the increment of plastic strains $\left\{d\varepsilon^2\right\}_t$ is determined using Equation (1). The components of the plastic strain tensor:$\left\{\varepsilon^P\right\}_t = \left\{\varepsilon^P\right\}_{t-1} + \{d\varepsilon^p\}_t$, the elastic strain $\{\varepsilon^y\}_t = \{\varepsilon\}_t - \left\{\varepsilon^P\right\}_t$, and the stress tensor $\{\sigma\}_t = [D] \cdot \{\varepsilon^y\}_t$, can then be determined. After that, the position of the yield surface is updated based on the refined values of plastic strains, and the described algorithm is repeated.

The iterative process is terminated when the condition, $\left\{d\varepsilon^P\right\}_t \leq \varepsilon_0.$, is met in all points of the considered domain.

The developed algorithm and the corresponding computational program were validated by solving a series of benchmark problems.

The accuracy of the approximate integration of expressions related to volumetric loads was verified by calculating the stresses caused by the self-weight of a homogeneous soil layer.

3.2. Design and bearing capacity assessment of pile foundations

Pile foundations are a fundamental structural component of fixed offshore platforms (FOPs). Depending on site conditions and project requirements, FOPs may utilize different types of pile installation techniques, including precast driven piles (installed using diesel hammers), vibro-driven piles (installed using vibratory drivers), and drilled-in piles.

It is well established that the critical axial load capacity of a pile is governed by two primary criteria: the bearing resistance of the surrounding soil and the structural strength of the pile material itself.

Currently, the ultimate axial bearing capacity of a pile with respect to soil resistance is determined using one or a combination of the following methods: full-scale load testing, analytical calculations based on geotechnical theory, empirical correlations, and dynamic formulae.

Among these, the method based on full-scale (trial) load testing is considered the most reliable. To ensure accurate determination of the required pile length and its safe load-bearing capacity, trial piles are installed and tested directly at the construction site, often under the same geological and hydrological conditions where the permanent piles will be placed. Additionally, selected piles may undergo control testing to confirm design assumptions.

In trial testing, static loads are typically applied using various techniques, allowing for the direct measurement of actual pile resistance under real geotechnical conditions. Despite its high reliability, this method is labor-intensive and time-consuming—particularly in offshore environments, where logistical and technical constraints are more pronounced.

In parallel, a number of theoretical approaches and analytical formulas presented in the geotechnical literature have proven effective for practical design purposes. These methods offer acceptable accuracy and are particularly advantageous during the preliminary design phase, enabling engineers to estimate pile performance prior to construction.

The dynamic method for estimating the critical resistance of piles provides an effective means to evaluate each pile individually and compare their performance under impact loading conditions. Nevertheless, such dynamic approaches have inherent limitations, as they are unable to comprehensively account for all factors influencing pile driving behavior and penetration resistance, particularly in heterogeneous or layered soil profiles.

Empirical methods for determining the ultimate load-bearing capacity of piles often yield results that are more closely aligned with those obtained from static load testing. These formulas allow for approximate evaluation of pile capacity based on parameters such as applied load, cross-sectional geometry, and penetration depth, provided that the distribution of end-bearing resistance and shaft friction along the pile's embedded length is known.

Using standardized data on tip resistance and shaft friction provided in national building codes and engineering guidelines, a calculation methodology was developed to assess the bearing capacity of pile foundations used in FOPs. However, this method is only applicable under the assumption that the pile tip depth and total length do not exceed 35 m.

In real-world offshore construction—particularly in deepwater zones or, in some cases, even in shallow water conditions—the total pile length often far exceeds this limit, reaching depths of 120–130 m. When pile lengths exceed 35 meters, the existing normative approach dictates

that the design resistance at the pile tip (end-bearing capacity) should be limited to the value corresponding to a 35 m depth, irrespective of the actual embedment. Similarly, for shaft resistance f_i acting on soil layers located below the 35 m depth, only a partial correction is applied Equations (16) and (17). For example, in cohesive soils (clays), the shaft resistance for depths up to 100 m is typically estimated using empirical adjustments or depth-dependent formulations. These constraints significantly reduce the accuracy of predicted load-bearing capacity in long-pile designs and highlight the need for more robust and depth-sensitive computational models that reflect actual geotechnical behavior at large embedment depths.

$$f_i = k_f f_{35} \tag{16}$$

where k_i is a coefficient accepted depending on the soil flow index, I_L;

$$\begin{cases} if\ I_L \le 0.4,\ then\ k_1 = 0.5 + 0.0143 h_i \\ if\ 0.4 < I_L \le 0.5,\ then\ k_i = 0.55 + 0.0125 h_i \\ if\ I_L > 0.5,\ then\ k_f = 0.65 + 0.01 h_i \end{cases} \tag{17}$$

where

- k_f refers to pile foundation stiffness;
- k_1 refers to soil stiffness coefficient;
- k_i refers to interfacial stiffness.

Here, h_i denotes the vertical distance (in meters) from the seabed to the midpoint of the i-th soil layer, while f_3 represents the design shaft resistance at a reference depth of 35 m. This value is determined based on the flow index of the i-th soil layer. For cohesive soils (such as clays) encountered at depths exceeding 100 m, the shaft resistance i-th is conventionally assumed to be equal to the design resistance at 100 meters, corresponding to the flow index of the respective layer. However, in such cases, the limiting condition $f_i \le 100\ kPa$ must be satisfied to ensure design consistency and avoid overestimation of the pile's load-bearing capacity.

It becomes evident that the design end-bearing resistance R at the pile tip is conservatively limited to the value corresponding to a 35 m depth, which does not reflect actual site conditions at greater depths. This simplification excludes geotechnical data beyond 35 m, resulting in inefficient use of available site-specific information and potentially unnecessary increases in construction time and cost. A similar issue arises in estimating the shaft resistance f, along the lateral surface of the pile, where values obtained at 35 m are inappropriately extended to depths up to 100 m without considering depth-dependent variations. Consequently, valuable *in situ* soil investigation data—acquired through detailed geotechnical surveys—remain underutilized in the design process, diminishing the reliability and efficiency of the foundation design.

As previously noted, empirical equations used to estimate the ultimate (or critical) load-bearing capacity of piles often yield results that are more consistent than those obtained from static load testing. Therefore, it is essential to incorporate laboratory and *in situ* test data to the fullest extent in order to improve the accuracy of these empirical approaches. In the case of tubular piles embedded in cohesive (clayey) soils, the shaft resistance along the pile's lateral surface should be evaluated using refined empirical expressions that take into account the specific geotechnical characteristics of the soil Equation (18).

$$f = \alpha\tau \tag{18}$$

where α is a dimensionless coefficient; τ is soil's shear force at the given investigated point.

The value of the coefficient α is determined using Equations (19) and (20).

$$\alpha = \frac{0.5}{\sqrt{\psi}} \text{ for } \psi \le 1.0 \tag{19}$$

$$\alpha = \frac{0.5}{\sqrt[4]{\psi}} for \psi > 1.0 \tag{20}$$

where the value of ψ is accepted for the given investigated point of the soil Equation (21).

$$\psi = \frac{\tau}{p_0^{'}} \tag{21}$$

where $p_0^{'}$ is the soil overload located above the investigated point to the soil surface.

As is seen from Equation (18), the shear force τ is the main parameter of the soil. The value of τ for cohesive soils, subjected to the mathematical expression of the Coulomb law, is determined by Equation (22).

$$\tau = c + \sigma tg\varphi \tag{22}$$

where c is the soil's adhesion force; φ is the soil's internal friction angle; and σ is normal pressure.

Equation (22) can be interpreted as stating that the ultimate shear resistance of cohesive soils is a linear function of the normal stress and comprises two components. The first component, denoted by, is independent of the normal pressure and reflects the intrinsic cohesion of the soil, commonly referred to as τ_{adh}. The second component, expressed as $tg\varphi$, is directly proportional

to the applied normal stress and represents the τ_{fr} of the soil.

In cases where shear deformations are minimal, the total shear resistance is governed predominantly by the cohesive term, which accounts for the adhesive forces within the soil structure. However, under conditions of significant deformation, the frictional component $\sigma tg\varphi$ becomes increasingly relevant and must be incorporated into the overall resistance model Equation (23).

$$\tau = \tau_{adh} + \tau_{fr} \tag{23}$$

However, in practice, it is highly difficult to distinguish the part of the shear resistance τ_{adh} independent of normal pressure (adhesion) and the part directly proportional to it (friction) τ_{fr}, as any change in pressure affects not only the second component but the first one as well. However, as the critical value of shear forces holds only at large deformations, this value practically makes it possible to determine $\tau_{cr.fr}$ Equation (24).

$$\tau_{cr.fr} = \tau_{cr} - \tau_{adh} \; or \; \tau_{cr.fr} = \tau_{cr} - c \tag{24}$$

For these values, the critical friction force along the lateral surface, according to Equation (18), is shown in Equation (25).

$$\tau_{cr.fr} = \alpha\,(\tau_{cr} - c) \tag{25}$$

Furthermore, accepting the depth of the pile foundation from the soil surface and the bulky weight in natural state γ_{soil}, the value of ψ from Equation (21) can be obtained using Equation (26).

$$\psi = (\tau_{cr} - c)/\gamma_{soil} h \tag{26}$$

The design value of the frictional resistance along the lateral surface of the pile foundation is determined based on the applied safety factor or specified working conditions, with the coefficient $\gamma_{\mathrm{cf}} = 0{,}5$. When calculating lateral friction forces, the soil-to-pile wall friction angle δ must be properly considered, as it significantly influences the interface shear resistance.

As established by experiment, the value of friction on the wall of the metal pile is less than the angle of the soil's inner friction of the ϕ. So, for example, depending on the type of soil, if $\phi = 35°$, then the value for pure sand, $^{\delta} = 15°$; for muddy sand, $\phi = 20°$ and $^{\delta} = 15°$; for sandy slit, $\phi = 25°$ and $^{\delta} = 20°$; and for sand, $\phi = 20°$, $^{\delta} = 15°$. For other types of soil, before obtaining experimental data, one can take these values equal to $\mathrm{tg}^{\delta} = \mathrm{tg}$ (ϕ - x°). The value of x° for different soils may be accepted as for clay soil, i.e., $\mathrm{x}° = 2° \div 3°$. Consequently, the design value of the friction force along the lateral surface of the pile foundation at the investigated point (layer), with regard to the above-stated one, is shown in Equation (27).

$$\left.\begin{array}{c} f_i = \frac{\gamma_{cf}\ \alpha(\tau_{cr}-c)tg\delta}{tg\varphi}, \psi = (\tau_{cr} - c)/\gamma_{soil} \cdot h \\ \alpha = 0.5\sqrt{\psi}, for\ \psi \le 1.0;\ \propto = 0.5\sqrt[4]{\psi}, for\ \psi > 1.0 \end{array}\right\} \tag{27}$$

To determine the design value of the friction force along the lateral surface of the pile foundation, we refer to data from laboratory research of soils for the fixed platform at Gunashli Field in the Caspian Sea. Soil samples for laboratory research were taken at a depth of $h = 25$ m. The data of laboratory research of the soil included: bulk weight of the soil $\gamma_{soil} = 19.6$ kN/m^3; critical shear force of the soil $\tau_{cr} = 90$ kPa, soil adhesion force $c = 20$ kPa; angle of inner friction of the soil $\phi = 17°45'$; consistency index $I_1 = 0{,}43$; and the type of the soil (gray layered clay with interlayers of fine sand).

The value of ψ is then determined using Equation (21). The f_i value is then obtained using Equation (27).

$$\psi = 90 - \frac{20}{19.6} x25 = 0.142 < 1.0$$

$$\propto = \frac{0.5}{\sqrt{\psi}} = \frac{0.5}{\sqrt{0.142}} = 1.33$$

$$f_i = \frac{\gamma_{cf}\alpha\,(\tau_{cr} - c)\,tg\left(\varphi - 2^{\circ}\right)}{tg\varphi} = 41.01\ kPa$$

At the same depth, for $I_L = 0.143$, the value of $f_i = 40.4$ kPa, which practically coincides with the value by building regulations. For the designed resistance of the soil R under the lower end (base) of the pile foundation, several methodologies have been proposed to estimate the load-bearing capacity of soils beneath foundations, wherein the geometry of the failure surface is assumed based on simplified conditions. In such models, the shape of the slip surface is postulated a priori, typically a compressed triangular failure wedge, resembling the form adopted in weightless soil conditions but with inclined boundaries adapted to accommodate non-horizontal base profiles.

In cases where the soil mass is wedge-shaped, the failure mechanism incorporates the mobilization of passive resistance along the boundaries of the wedge. This resistance is often computed using approximate expressions derived for assumed slip-line contours within radial shear zones, frequently estimated by logarithmic spirals. These assumptions are primarily applicable within the

framework of plane–strain analysis and rely on the global convexity of the failure mechanism.

To extend such estimations to practical applications involving square or circular foundations, empirical correction coefficients are introduced to account for deviations from idealized conditions, including 3D effects and internal shear contributions. It is important to highlight that progress has been made in developing rigorous solutions grounded in the theory of limit equilibrium. In particular, a robust and flexible method for solving the governing differential equations of limit equilibrium has been formulated, enabling the derivation of solutions with controllable accuracy for various boundary conditions.

Moreover, the differential formulation for axisymmetric failure conditions has been resolved for a predefined slip surface geometry. Under these assumptions, circular and square foundations may be treated as rigid bodies, maintaining the equilibrium of the compressed failure core, and their ultimate bearing capacity can be evaluated using a general expression Equation (28).

$$R = \frac{N_{\nu k}\gamma_{soil}D}{2} + N_{qk}\gamma_{soil}h + N_{ck}c \qquad (28)$$

where N_{vk}, N_{qk}, and N_{ck} are dimensionless quantities dependent on the soil's inner friction angle, and are called the load-carrying factors (Table 1); γ_{soil} is the bulky mass of the soil in the natural state; D is the diameter of the pile foundation; h is the foundation depth of the pile foundation counted from the base to the surface of the soil; C is the soil adhesion force.

Using the data of soils for the previous example, the design value of the soil resistance R under the lower end of the pile at a depth of 25 m can be calculated. Accepting the diameter of the cross-section equal to $D = 1.4$ m and using the tabular values for the inner friction angle $\phi = 17°45'$, we determine $N_{vk} = 5.3$, $N_{qk} = 6.0$, and $N_{ck} = 15.8$. Consequently, $R = 3328.7$ kPa.

For the value $I_L = 0{,}43$ by building regulations, the design resistance under the lower end of pile foundations at a depth of 25 m is $R = 3035$ kPa. In this case, the offered Equation (28) yields an 8% overestimation relative to the data from building regulations.

Accordingly, the calculation of the load-bearing capacity of a pile foundation is carried out by applying the refined design Equation (27) to evaluate the lateral soil resistance f_i for each individual layer, and Equation (28) to determine the end-bearing resistance R at the pile tip. These are complemented by the use of standard design methodologies outlined in national building codes and All-Union construction regulations.

To ensure the reliability and representativeness of laboratory-based assessments of the soil's design resistance along the pile shaft, it is essential to subdivide the soil profile into geotechnically homogeneous strata, each with a maximum thickness of 2 m. This stratification enables accurate integration of laboratory findings into the design framework and enhances the precision of bearing capacity estimations under variable subsurface conditions.

Given the unique operational characteristics of pile foundations beneath storage tanks, bearing capacity was evaluated through static load testing under axial compressive force. The reaction system employed anchor piles positioned along the same radial beam as the test pile, symmetrically arranged on both sides. Neither the anchor piles nor the tested pile was connected to the conductor block during the testing phase, ensuring isolated load application.

The anchor piles were rigidly linked via a thrust beam composed of two I-beams (type No. 60), which were responsible for resisting the counteracting forces generated by the hydraulic jacks. With a span of 3500 mm and a maximum test load of 2000 kN, the resulting mid-span deflection did not exceed 5 mm, corresponding to approximately 0.0014 of the total span, which was well within acceptable limits for structural rigidity.

The static loading of the test piles was performed using a hydraulic system comprising two DG-150 jacks, each with a lifting capacity of 1,500 kN, connected to an NSP-400 hydraulic power unit. The magnitude of the applied load was controlled via an MO-400 analog pressure gauge, featuring a measurement range of up to 40 MPa and a resolution of 0.2 MPa. The hydraulic jacks were positioned atop a steel loading frame affixed to the pile head, ensuring uniform load transfer during testing.

Reaction forces generated by the jacks were transmitted through a system of rigid thrust beams designed to minimize deformation and maintain alignment during the test procedure. The scheme of the static load tests is illustrated in Figure 2.

Although the overall load-displacement response of the pile–soil interaction exhibited elastic–plastic behavior (Figure 3), the influence of viscous effects—while generally minimal during dynamic loading—can be incorporated into the model for improved accuracy in

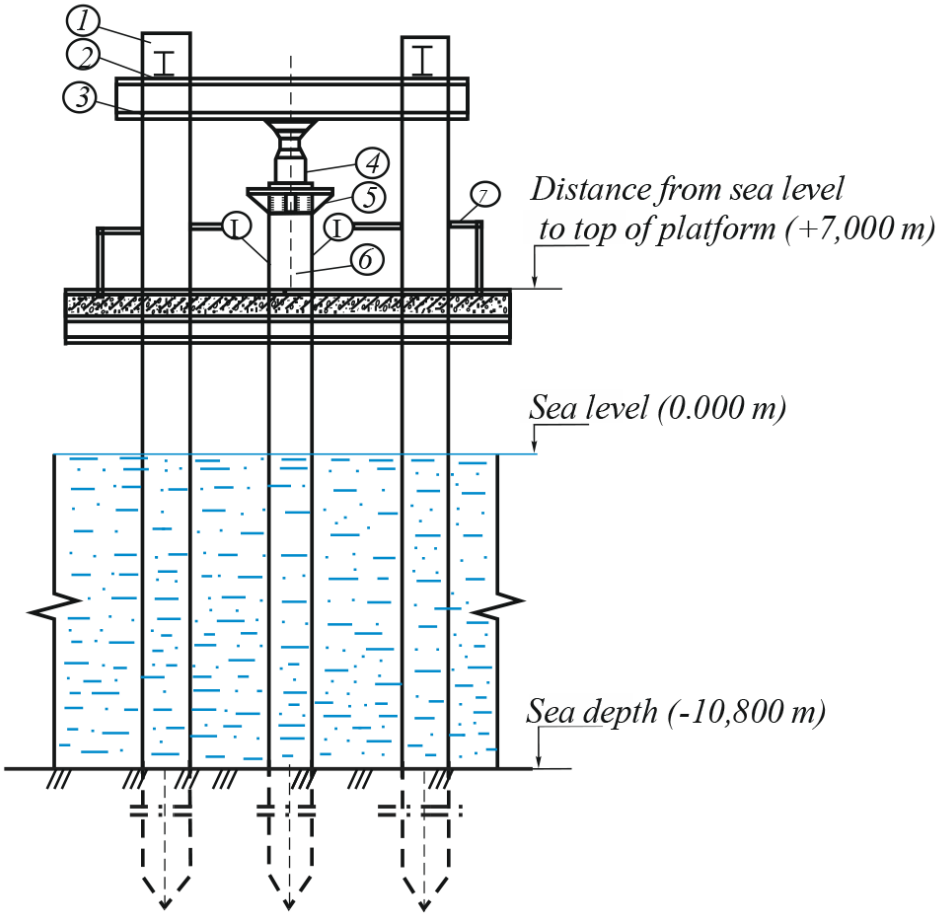

Figure 2. Scheme of installations for static pile testing
Notes: 1: Anchor piles; 2: Distribution beams; 3: Over jack support beam; 4: Jack-1,500–2,000kN; 5: Jack table; 6: Test pile; 7: Reference system with deflection gauges.

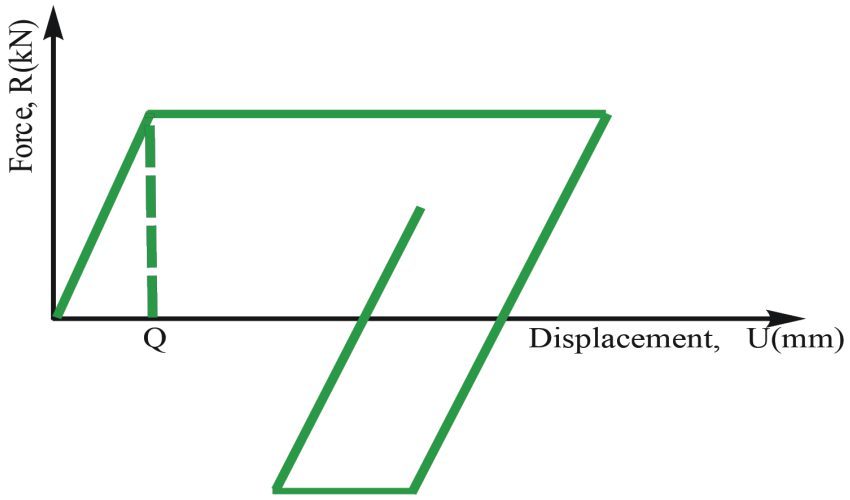

Figure 3. Diagram of the dependence of resistance on total displacements of the pile and the soil
Notes: Q: The total load applied to the pile, measured in kilonewtons (kN); R: The resistance provided by the pile against the applied load, measured in kilonewtons (kN); U: The displacement of the pile under the applied load, measured in millimeters (mm).

Table 1. Values of characteristic exponents of the cement stone strength in calculating the pile foundations' strength and stability

$\varphi(^\circ)$	N_{uk}	N_{qr}	N_{cr}	$\varphi(^\circ)$	N_{uk}	N_{qr}	N_{cr}
16	4.10	4.50	12.80	29	29.95	28.80	50.20
17	4.90	5.50	14.80	30	34.60	32.80	55.40
18	5.70	6.50	16.80	31	41.70	39.15	63.50
19	6.50	7.50	18.85	32	48.80	45.50	71.50
20	7.30	8.50	20.90	33	59.00	54.80	82.60
21	8.60	9.65	22.80	34	69.20	64.00	93.60
22	9.90	10.80	24.60	35	83.20	75.80	106.80
23	11.95	12.45	27.25	36	97.20	87.60	120.00
24	14.00	14.10	29.90	37	119.80	107.30	140.50
25	16.45	16.35	33.20	38	142.50	127.00	161.00
26	18.90	18.60	36.40	39	179.00	156.00	190.00
27	22.10	21.70	40.70	40	216.00	185.00	219.00
28	25.30	24.80	45.00				

capturing time-dependent resistance characteristics.

Thus, a robust scientific and methodological framework was established based on one-dimensional wave propagation theory, enabling detailed analysis of long pile driving processes. This approach allowed the assessment of stress–strain state at any stage of the hammer–pile–soil interaction and provided a reliable estimate of the pile's total load-bearing capacity. The method was implemented in an automated computational algorithm, and as a result, a characteristic curve (Figure 4) was generated, representing the variation in pile resistance relative to the number of hammer blows required to reach a specific embedment depth.

To validate and refine the proposed methodology, both static and dynamic load tests were conducted on seven piles installed in various locations across the Caspian Sea. These tests were conducted under varying site conditions and seabed depths to evaluate the performance and applicability of the model. The outcomes of these experimental investigations are illustrated in Figure 5–7. Information about the hammer–pile–soil system and the results of the tests is shown in Table 2.

As a result of the present investigation, a functional relationship was established between the soil resistance acting on the pile and the number of hammer blows per unit penetration length, taking into account the specific characteristics of the selected hammer type and pile geometry.

As illustrated in Table 2, the load-bearing capacities of the test piles estimated using conventional building code formulas were 7–16% lower than those obtained from static load tests. Conversely, the results from the dynamic method exceeded those of the static test by 19–48%. Moreover, observations made during both static and dynamic test procedures revealed several phenomena not accounted for in theoretical models. Notably, it was observed that internal soil plugs within piles shorter than 30 m (∅377 × 11 mm and ∅426× 11 mm) continued to develop and compact progressively throughout the driving process. This suggests that such piles behave as open-ended during installation, yet exhibit the characteristics of closed-end piles under static loading, once the specified set of criteria is met. The geotechnical profile at the test site comprised a 1 m-thick surface layer of cockle-shell-mixed sand, underlain by approximately 20 m of fine grey sand, followed by stiff clay interbedded with brown sandstone fragments.

The results of the comparison of the forecasting capacity of the load-bearing capacities for the tested piles are shown in Table 3.

As shown in Table 3, the predicted load-bearing capacities obtained using building code methods (both approaches) deviate from the actual pile capacities by approximately 30–40%. The calculation method based on building code tables exhibits a relatively large root-mean-square error, whereas the dynamic method tends to significantly overestimate the load-bearing capacity. Moreover, the higher standard deviation values associated with the building code methods indicate that these approaches are not fully reliable, highlighting the need for further research to improve prediction accuracy.

The main findings of this study, including the bearing capacity and settlement behavior of pile

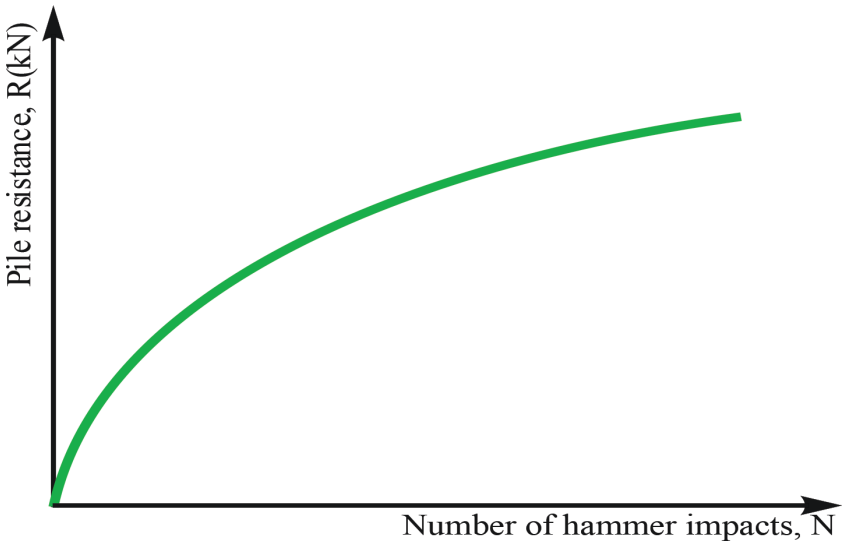

Figure 4. The graph of the dependence of the pile's load-bearing capacity with respect to soil on the number of impacts of the hammer
Notes: N: Number of impacts of the hammer; R: Pile resistance.

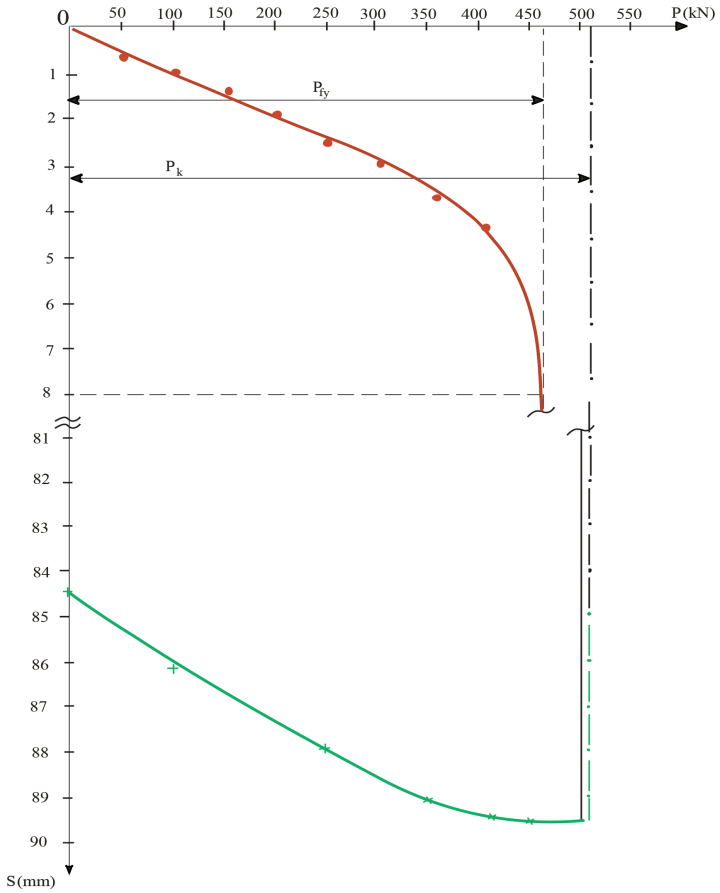

Figure 5. Loading schedule for piles with a diameter of 377 × 11 mm
Notes: Red dot (·): Pile-loading steps; ×: Pile-unloading steps; P: The total applied load on the pile, measured in kilonewtons (kN); P_k: Critical load on piles; P_{fy}: Actual load-bearing capacity of piles depending on soil; .

foundations considering soil plasticity, are presented in a comparative format in the **Graphical Abstract.**

4. Discussion

From a theoretical standpoint, the proposed method is grounded in solving the one-dimensional dynamic problem of force propagation within the hammer–pile–soil system using numerical techniques, specifically the FEM.

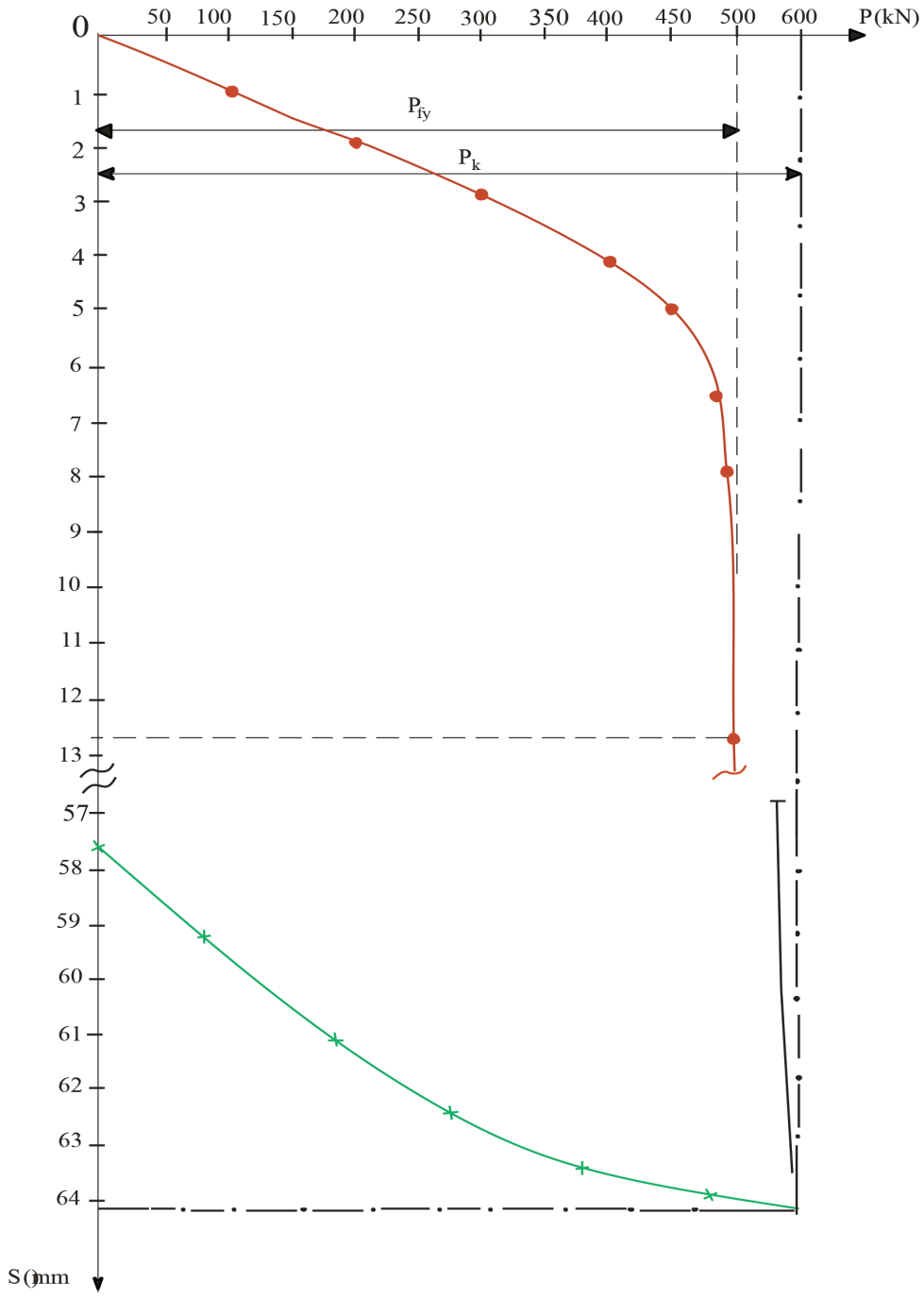

Figure 6. Loading schedule for piles with a diameter of 426 × 11 mm
Notes: Red dot (·): Pile-loading steps; ×: Pile-unloading steps; P: The total applied load on the pile, measured in kilonewtons (kN); P_k: Critical load on piles; P_{fy}: Actual load-bearing capacity of piles depending on soil; S: The displacement of the pile under the applied load, measured in millimeters (mm).

To overcome the analytical challenges posed by the complex physical and mechanical behavior of soils, the hammer–pile–soil interaction is modeled using discrete elements characterized by their constitutive relations—elastic, plastic, and viscous (Figure 1). Although the pile–soil resistance typically exhibits an elastic–plastic behavior, the model also allows for the incorporation of viscous effects, which, although minor, may influence the response during high-strain-rate impact loading. The analysis confirmed that ignoring plastic deformation can lead to overestimated bearing capacity and underestimated settlement, potentially compromising structural safety. This highlights the need for updating existing calculation methods to incorporate nonlinear soil behavior.

From a practical standpoint, the computational cost, ease of implementation, and compatibility with widely adopted engineering software and standards are crucial factors. The proposed method demonstrates both numerical efficiency

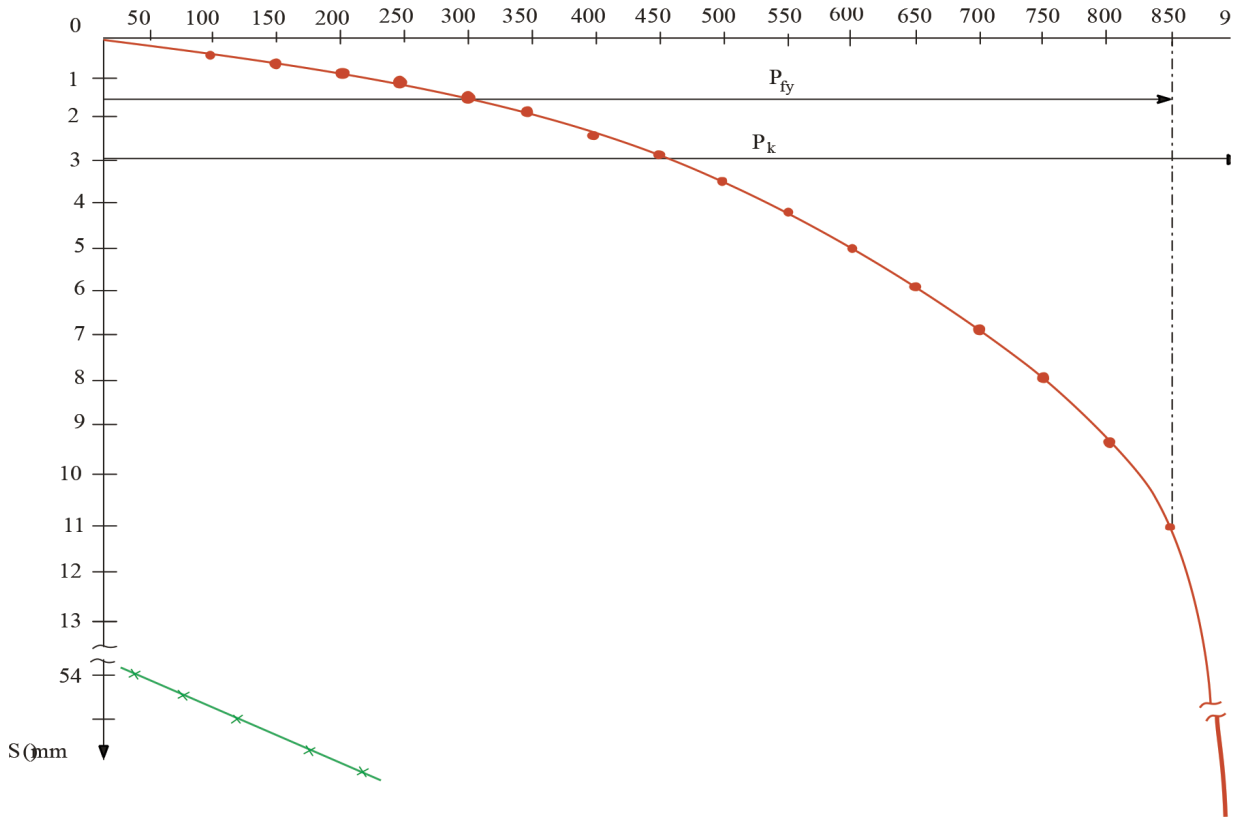

Figure 7. Loading schedule of piles with a hard core
Notes: Red dot (·): Pile-loading steps; ×: Pile-unloading steps; P: The total applied load on the pile, measured in kilonewtons (kN); P_k: Critical load on piles; P_{fy}: Actual load-bearing capacity of piles depending on soil; S: The displacement of the pile under the applied load, measured in millimeters (mm).

Table 2. The spiral movement of piles in soil during the driving process

Piles number	**1**	**2**	**3**	**4**	**5**	**6**	**7**
Dimensions of the piles							
Cross-section diameter (mm)	377 × 11	426 × 11	377 × 11	377 × 12	377 × 12	377 × 11	426 × 12
Total length (m)	24.3	25.0	27.4	27.0	27.0	25.0	23.0
Driving depth (m)	6.00	6.00	8.20	12.25	11.50	8.00	7.00
Indicators of the hammer							
Total mass (kN)	25	25	25	24	24	24	24
Elevation height (m)	1.8–2.0	1.8–2.0	1.8–2.0	1.8–2.0	1.8–2.0	2.0	2.0
Rejection (mm)	1.5	1.5	1.5	2.0	2.5	2.6	2.5
Test results							
Static resistance of the pile (kN)	510	560	918	920	840	895	800
Compared to static resistance on building regulations	0.84	0.89	0.85	0.90	0.93	0.89	0.86
Compared to static resistance by the dynamic method	1.25–1.34	1.31–1.46	1.29–1.41	1.24–1.43	1.19–1.36	1.27–1.39	1.34–1.48

and compliance with recognized regulatory frameworks, making it suitable for real-world offshore engineering applications.

5. Conclusion

A scientifically grounded, methodologically practical framework was developed based on one-dimensional wave theory to analyze the driving process of long piles, evaluate the stress–strain behavior at any stage of hammer–pile–soil interaction, and accurately estimate the total load-bearing capacity of the pile. The assessment of pile bearing capacity following installation is performed using a wave-impact approach, with the numerical solution implemented via the FEM.

A key outcome of this study is the demonstration that, under appropriate initial conditions, the developed method enables the prediction of

Table 3. Comparison of the tested traces

Types of soils	Forecast methods (δ)			
	By building code	Dynamical method (building code)	Limit friction method	API
Consolidated clays	$\frac{0.726}{0.537}$	$\frac{1.326}{0.487}$	$\frac{1.116}{0.208}$	$\frac{1.011}{0.218}$
Solid plastic clays	$\frac{0.683}{0.410}$	$\frac{1.421}{0.399}$	$\frac{1.032}{0.197}$	$\frac{0.991}{0.319}$
Other rocks	$\frac{0.917}{0.511}$	$\frac{1.371}{0.364}$	$\frac{0.964}{0.121}$	$\frac{0.927}{0.284}$

Note: δ: Mean square difference.
Abbreviation: API, American Petroleum Institute.

pile bearing capacity even in the absence of detailed information on the physical and mechanical properties of the soil. In this context, the pile body functions as an *in* probe, enabling evaluation of the total soil resistance encountered per unit length during each impact cycle.

It is recommended that design values of soil resistance—both along the shaft and at the toe—be determined for embedment depths exceeding 35 m. In parallel with the dynamic assessment, a control calculation should be carried out based on geotechnical investigations and laboratory test data to ensure reliability. By modeling soil resistance along the shaft using elastic–plastic elements, the relationship between resistance and total displacement of the pile–soil system can be more accurately defined.

The bearing capacity of piles was assessed using both code-based procedures and empirical methods, considering various soil types. The average ratio of calculated to experimentally determined load-bearing capacities, and the associated root-mean-square error, were determined. Furthermore, the energy transfer coefficient, which plays a critical role in driven pile performance, was derived through comparative analysis of static and dynamic testing results. It was observed that this coefficient is highly sensitive to several factors, such as hammer drop height, pile head configuration, pile flexibility, and the elastic properties of the surrounding soil.

Finally, the study established a predictive relationship between pile resistance and the number of hammer blows per unit depth for a given pile–hammer system, contributing to the optimization of pile installation and performance evaluation in complex geotechnical environments.

The study confirmed that accounting for soil plasticity yields more realistic and reliable results. This methodology is recommended for future offshore foundation design to ensure consistency with actual ground conditions.

The main findings of this study, including the bearing capacity and settlement behavior of pile foundations considering soil plasticity, are succinctly presented in the **Graphical Abstract**.

Acknowledgments

None.

Fundings

None.

Conflict of interest

The authors declare they have no competing interests.

Author contributions

Conceptualization: All authors
Methodology: All authors
Investigation: All authors
Writing–original draft: Latif F. Aslanov
Writing–review & editing: Ulvi L. Aslanli

Availability of data

Data are publicly available.

AI tools statement

All authors confirm that no AI tools were used in the preparation of this manuscript.

References

1. Alekseev AG, Bezvolev SG. Determination of the bearing capacity of a helical pile using screwing torque considering shaft geometry. *Soil Mech Found Eng.* 2023;60:189–197. https://doi.org/10.1007/s11204-023-09881-4
2. Alzabeebee S, Ismael BH, Keawsawasvong S, Alshami AW. An evolutionary polynomial computing of pile capacity using the results of high-strain dynamic test. *Transp Infrastruct Geotechnol.* 2024;11,3160–3177. https://doi.org/10.1007/s40515-024-00411-9

3. Angurana DI, Yadav JS, Khatri VNK. Estimation of uplift capacity of helical pile resting in cohesionless soil. *Transp Infrastruct Geotechol.* 2024;11(2):833–864. https://doi.org/10.1007/s40515-023-00299-x
4. Armaghani DJ, Harandizadeh H, Momeni E, Maizir H, Zhou J. An optimized system of GMDH-ANFIS predictive model by ICA for estimating pile bearing capacity. *Artif Intell Rev.* 2022;55:2313–2350. https://doi.org/10.1007/s10462-021-10065-5
5. Aslanov LF. Wave interaction of offshore structure and shelf soil through large section piles with a 'hard core' on the half-space model. *Neft Khozyaystvo.* 2015;2:78-81.
6. Aslanov LF. Interaction between large cross-sections bored piles with 'hard core' under dynamic loads and shelf soils. *Sci Bull Natl Min Univ.* 2015;5:21-25.
7. Aslanov LF. Reflected wafes from bored or CFA piles of large section in the offshore soils. *Neft Khozyaystvo.* 2016;7:112-116.
8. Aslanov LF. Optimization of the calculation of the piles of fixed offshore platforms. In: El-Askary H, Erguler ZA, Karakus M, Chaminé HI, eds. *Research Developments in Geotechnics, Geo-Informatics and Remote Sensing. CAJG 2019. Advances in Science, Technology & Innovation.* Cham: Springer; 2022. https://doi.org/10.1007/978-3-030-72896-0_32
9. Aslanov LF, Aslanli UL. Study of the stress-strain state of the pontoon element of the support block. *SOCAR Proc.* 2024;2:115-121. https://doi.org/10.5510/OGP20240200976
10. Aslanov LF, Aslanli UL. Study of marine hydraulic structures under seismic effects. In: Ksibi M, et al. *Recent Advances in Environmental Science from the Euro-Mediterranean and Surrounding Regions (4th Edition). EMCEI 2022. Advances in Science, Technology & Innovation.* Cham: Springer; 2024. https://doi.org/10.1007/978-3-031-51904-8_193
11. Aslanov LF, Aslanli UL. Determination of load-bearing capacity of piles used in stationary offshore platforms. *SOCAR Proc.* 2024;1:116-123. https://doi.org/10.5510/OGP240100949
12. Aslanov LF, Aslanov FL. Choosing an effective design solution for fixing offshore hydro-technical structures to shelf ground. In: Çiner A, et al. *Recent Research on Geotechnical Engineering, Remote Sensing, Geophysics and Earthquake Seismology. MedGU 2021. Advances in Science, Technology & Innovation.* Cham: Springer; 2024. https://doi.org/10.1007/978-3-031-43218-7_22
13. Aslanov LF, Aslanov FL. Some tasks of increasing and identifying the reserves of the bearing capacity of anchor fastenings of offshore fixed platforms. In: Bezzeghoud M, et al. *Recent Research on Geotechnical Engineering, Remote Sensing, Geophysics and Earthquake Seismology. MedGU 2022. Advances in Science, Technology & Innovation.* Cham: Springer; 2024. https://doi.org/10.1007/978-3-031-48715-6_10
14. Aslanov LF, Aslanli UL, Aslanov FL. Construction of foundations for reservoirs in the Caspian Sea. *SOCAR Proc Special Issue No. 1.* 2024;29-38. https://doi.org/10.5510/OGP2024SI101031
15. Aslanov LF, Aslanli UL, Aslanov FL. New calculation method for the pontoon element of offshore fixed platforms for oil and gas production. *Nafta-Gaz 2025.* 2025;(3):188–198. https://doi.org/10.18668/NG.2025.03.05
16. Bokov IA, Fedorovskii VG. Taking into account the soil depth inhomogeneity in calculation of the piles settlement. *Soil Mech Found Eng.* 2021;58(4):267–272. https://doi.org/10.1007/s11204-021-09738-8
17. Buragadda V, Orekanti ER. Predicting the allowable settlement of reinforced soil foundations: a laboratory study. *Geotech Geol Eng.* 2024;42(3):2271–2291. https://doi.org/10.1007/s10706-023-02637-9
18. Campione G. Influence of shallow foundations on the response of steel wind towers. *Int J Civ Eng.* 2024;22(1):1309–1319. https://doi.org/10.1007/s40999-023-00936-z
19. Chaabani H, Mesmoudi S, Boutahar L, El Bikri K. Buckling of porous FG sandwich plates subjected to various non-uniform compressions and resting on Winkler–Pasternak elastic foundation using a finite element model based on the high-order shear deformation theory. *Acta Mech.* 2022;233,5359–5376. https://doi.org/10.1007/s00707-022-03388-z
20. Chen S, Chen X. Estimation of pile bearing capacity using hybrid models based on modified radial base function. *Multiscale Multidiscip Model Exp Des.* 2024;7:5347-5363. https://doi.org/10.1007/s41939-024-00523-2

21. Chen SS, Kao CJ, Shi JY. Dynamic analysis of cylindrical foundations under torsional loading via generic discrete-element models simulating soil stratum. *Sci Rep.* 2023;13(1):19163. https://doi.org/10.1038/s41598-023-46046-7
22. Chimdesa FF, Chimdesa FF, Jilo NZ, et al. Numerical analysis of pile group, piled raft, and footing using finite element software PLAXIS 2D and GEO5. *Sci Rep.* 2023;13(1):15875. https://doi.org/10.1038/s41598-023-42783-x
23. Kim D. Analysis on lateral resistance of precast bored piles based on experimental and numerical approach. *Geomech Eng.* 2025;41(2):319-325. https://doi.org/10.12989/gae.2025.41.2.319. (Special Issue).
24. Dubrakova K, Bulgakov A, Bock T. Determination of homogeneous foundation's settlement based on the integral estimation method. In: Vatin N, Pakhomova EG, Kukaras D, eds. *Modern Problems in Construction. Lecture Notes in Civil Engineering, vol 287*. Cham: Springer; 2023. https://doi.org/10.1007/978-3-031-12703-8_29
25. Fattah MY, al-Omari RR, Kallawi AM. Load sharing between shaft and tip of pile group in saturated and unsaturated soil. *Transp Infrastruct Geotechol.* 2024;11(4):2117–2147. https://doi.org/10.1007/s40515-023-00366-3
26. Feng SJ, Xi W, Zhang XL, Sun DM. Experimental and numerical investigations on the mechanical response of full-scale PHC pile foundations for solar power generation. *Acta Geotech.* 2024;19:5293–5314. https://doi.org/10.1007/s11440-024-02257-4
27. Gang L. Improving the estimation of the pile bearing capacity via hybridization technique based on adaptive network based fuzzy inference. *J Ambient Intell Human Comput.* 2024;15:4043–4060. https://doi.org/10.1007/s12652-024-04878-9
28. Gotman NZ, Evdokimov AG. Calculation of bridge-support pile foundations taking karst deformations into account in the base. *Soil Mech Found Eng.* 2023;60:401–409. https://doi.org/10.1007/s11204-023-09908-w
29. Hadi AI, Sunaryo, Farid M, et al. (2024). Analysis of earthquake-prone areas based on the seismic wave velocity, Y oung's modulus, shear modulus, and Poisson's ratio for disaster risk reduction in Bengkulu city, Indonesia. *Nat Hazards.* 2024;120:14683-14702. https://doi.org/10.1007/s11069-024-06827-3
30. Xia H, Du G, Cai J, Sun C. Model tests on the bearing capacity of pervious concrete piles in silt and sand. *Geomech Eng.* 2024;38(1):079-91. https://doi.org/10.12989/gae.2024.38.1.079
31. Hassona F, Hakeem BM. Numerical investigation of the carrying capacity of single polyurethane foam pile in clay and sand soils. *J Umm Al-Qura Univ Eng Archit.* 2024;15:78–92. https://doi.org/10.1007/s43995-023-00043-z
32. He P, Deshpande V, Newson T. Undrained capacity of shallow octagonal foundations under combined VHM loading. *Geotech Geol Eng.* 2023;41:1275–1286. https://doi.org/10.1007/s10706-022-02334-z
33. He L, Chen X, Wang Z, et al. A case study on the bearing characteristics of a bottom uplift pile in a layered foundation. *Sci Rep.* 2022;12:22457. https://doi.org/10.1038/s41598-022-27105-x
34. Heidarie Golafzani S, Eslami A, Jamshidi Chenari R, Hamed Saghaian M. Optimized selection of axial pile bearing capacity predictive methods based on multicriteria decision-making (MCDM) models and database approach. *Soft Comput.* 2022;26:5865–5881. https://doi.org/10.1007/s00500-021-06583-7
35. Hoang VNV, Thanh PT. Influence of nonuniform elastic foundations on free vibration behavior of nanocomposite plates interacting with a fluid environment based on a novel shear deformation theory. *Acta Mech.* 2024;235:4607–4637. https://doi.org/10.1007/s00707-024-03965-4
36. Huded PM, Dash SR. Pile foundation in alternate layered liquefiable and nonliquefiable soil deposits subjected to earthquake loading. *Earthq Eng Eng Vib.* 2024;23:359–376. https://doi.org/10.1007/s11803-024-2241-0
37. Jin J, Liu Y, Liu FX, Wang YF. Effects of combined loadings on the bearing performance of a typical pile foundation. *Mech Solids.* 2022;57:352–369. https://doi.org/10.3103/S0025654422020066
38. Kalinin A, Prolygin A, Aleksandrov N. Substantiation of the method for calculating soil deformation modulus. In: Mottaeva A, ed. *Technological Advancements in Construction. Lecture Notes in Civil Engineering, vol 180*. Cham: Springer; 2022:71-51. https://doi.org/10.1007/978-3-030-83917-8_7

39. Lee K, Kim M, Hwang T. Reinforcement effect of micropile and bearing characteristics of micropiled raft according to the cohesion of soil and stiffness of pile. *Geomech Eng.* 2024;37(5):511-525. https://doi.org/10.12989/gae.2024.37.5.511
40. Kong G-q, Liu Z-p, Wang L-h, Liu H-l, Yang Q. Experimental studies on the behavior of a single shaped pile under oblique pullout loads. *Acta Geotech.* 2023;18:4733–4746. https://doi.org/10.1007/s11440-023-01849-w
41. Kumar M, Kumar DR, Khatti J, Samui P, Grover KS. Prediction of bearing capacity of pile foundation using deep learning approaches. *Front Struct Civ Eng.* 2024;18:870–886. https://doi.org/10.1007/s11709-024-1085-z
42. Lai VQ, Shiau J, Keawsawasvong S, Tran DT. Bearing capacity of ring foundations on anisotropic and heterogenous clays: FEA, NGI-ADP, and MARS. *Geotech Geol Eng.* 2022;40:3913–3928. https://doi.org/10.1007/s10706-022-02117-6
43. Mahmood A, Alshameri B, Khalid MH, Jamil SM. Comparative study of various interpretative methods of the pile load test. *Innov Infrastruct Solut.* 2022;7:102. https://doi.org/10.1007/s41062-021-00697-5
44. Majumder M, Chakraborty D. Three-dimensional numerical analysis of under-reamed pile in clay under lateral loading. *Innov Infrastruct Solut.* 2021;6:55. https://doi.org/10.1007/s41062-020-00428-2
45. Maralapalle VC, Hegde R. Experimental and empirical study on piles socketed into the rock. *Soil Mech Found Eng.* 2024;61:56–61. https://doi.org/10.1007/s11204-024-09943-1
46. Mellal F, Bennai R, Avcar M, Nebab M, Hassen AA. On the vibration and buckling behaviors of porous FG beams resting on variable elastic foundation utilizing higher-order shear deformation theory. *Acta Mech.* 2023;234:3955–3977. https://doi.org/10.1007/s00707-023-03603-5
47. Soomro MA, Xiong S, Mangnejo DA, Karira H, Darban SA. Evaluating the interaction between tunnel excavation and battered piles: effects of depth and position using 3D numerical analysis. *Geomech Eng.* 2025:40(6):395-410. https://doi.org/10.12989/gae.2025.40.6.395
48. Soomro MA, Zhu Z, Darban SA, Cui ZD. A machine learning approach for predicting the impact of normal fault ruptures on batter pile foundations. *Geomech Eng.* 2025;40(3):193-204. https://doi.org/10.12989/gae.2025.40.3.193
49. Murali AK, Tran KM, Haque A, Bui HH. Experimental and numerical investigation of the load-bearing mechanisms of piles socketed in soft rocks. *Rock Mech Rock Eng.* 2022;55, 5555–5576. https://doi.org/10.1016/j.ultsonch.2022.105909
50. Mangi N, Su Q, Zhang Z, Pei Y, Luo A. Assessing the influence of sequential basement excavation and tunneling on a pile in stiff clay: a 3D coupled consolidation approach. *Geomech Eng.* 2025;40(5):379-393. https://doi.org/10.12989/gae.2025.40.5.379
51. Nguyen TH, Nguyen KVT, Ho VC, Nguyen DD. Efficient hybrid machine learning model for calculating load-bearing capacity of driven piles. *Asian J Civ Eng.* 2024;25(1):883–893. https://doi.org/10.1007/s42107-023-00818-8
52. Pantelidis L. The equivalent modulus of elasticity of soil mediums for designing shallow foundations. *Geotech Geol Eng.* 2021;39:3863–3873. https://doi.org/10.1007/s10706-021-01732-z
53. Pham TA, Nguyen DH, Duong HAT. Development of deep learning neural network for estimating pile bearing capacity. In: Ha-Minh C, Tang AM, Bui TQ, Vu XH, Huynh DVK, eds. *CIGOS 2021, Emerging Technologies and Applications for Green Infrastructure. Lecture Notes in Civil Engineering, vol 203.* Singapore; Springer; 2022. https://doi.org/10.1007/978-981-16-7160-9$_1$83
54. Roohi M, Faeli M, Irani M, Shamsaei E. Calculation of land subsidence and changes in soil moisture and salinity using remote sensing techniques. *Environ Earth Sci.* 2021;80(12):423. https://doi.org/10.1007/s12665-021-09723-2
55. Sharafutdinov RF, Razvodovskii DE, Zakatov DS. Single bored pile settlement prediction taking into account the elastic-plastic behavior of the soil. *Soil Mech Found Eng.* 2024;61:213–222. https://doi.org/10.1007/s11204-024-09965-9
56. Shen Y. Optimized systems of multi-layer perceptron predictive model for estimating pile-bearing capacity. *J Eng Appl Sci.* 2024;71:52. https://doi.org/10.1186/s44147-024-00386-x

57. Shubham K, Metya S, Sinha AK. Surrogate model-based prediction of settlement in foundation over cavity for reliability analysis. *Transp Infrastruct Geotechol.* 2024;11;1294–1320. https://doi.org/10.1007/s40515-023-00329-8
58. Sidorov VV, Le DA. Investigations of soil models used to study soil base liquefaction. *Soil Mech Found Eng.* 2024;61:138–144. https://doi.org/10.1007/s11204-024-09954-y
59. Singh M, Viladkar MN, Shekhawat PS, Tripathi K, Amin M. Bearing capacity of strip footings on jointed rock mass. *Arab J Geosci.* 2022;15:1579. https://doi.org/10.1007/s12517-022-10841-9
60. Sofiyev AH, Turan F, Kadıoglu F, Aksogan O, Hui D. Influences of two-parameter elastic foundations on nonlinear free vibration of anisotropic shallow shell structures with variable parameters. *Meccanica.* 2022;57:401–414. https://doi.org/10.1007/s11012-021-01439-8
61. Swarnkar DC, Singh AK, Shubham K. Application of ANN for prediction of settlement of ring foundation. *SIViP.* 2024;18:7537–7554. https://doi.org/10.1007/s11012-021-01439-8
62. Verumandy K, Arulrajah A, Mirzababaei M, Rajeev P. Static load testing of instrumented screw piles in soft soil deposits. *Int J Geosynth Ground Eng.* 2024;10:10. https://doi.org/10.1007/s40891-023-00519-x
63. Li W, Gong W, Dai G. Geomechanics and engineering, development and experimental validation of P-Y curves for rectangular piles. *Geomech Eng.* 2024:39(5):475-482. https://doi.org/10.12989/gae.2024.39.5.475
64. Wibowo LSB, Pradono MH, Fauzi HA, Sudarmadi S, Arman A, Perkasa M. Seismic behavior for reinforced concrete building due to foundation settlement on different soil types. *Iran J Sci Technol Trans Civ Eng.* 2024;48:861–870. https://doi.org/10.1007/s40996-023-01178-8
65. Wu W, Wang G, Wang L Hao R, Wang Y, Niu Q. Analysis of surface vibration response induced by PHC piles driven into non-uniform saturated soil layer. *Mech Solids.* 2024;59:813-830. https://doi.org/10.1134/S0025654423602264
66. Wu W, Wang G, Wang L, Wang Y, Hao R, Liu W. Dynamic response analysis of non-uniform unsaturated soil layer roadbed under uniform moving load. *Mech Solids.* 2024;59:280–296. https://doi.org/10.1134/S0025654423602197
67. Xiao L, Du K. Evaluation of driven piles' load capacity by optimization-based prediction algorithms. *Int J Interact Des Manuf.* 2025;19:3277–3288. https://doi.org/10.1007/s12008-024-01890-3
68. Yaychi BM, Esmaeili-Falak M. Estimating axial bearing capacity of driven piles using tuned random forest frameworks. *Geotech Geol Eng.* 2024;42(8):7813-7834. https://doi.org/10.1007/s10706-024-02952-9
69. Yuan WH, Wang HC, Li YJ, Zhnag W, Liu K. Large deformation assessment of the bearing capacity factor for rigid footing: effect of soil heterogeneity. *Comp Part Mech.* 2024;11(19). https://doi.org/10.1007/s40571-024-00763-6
70. Zhang A, Dieudonné AC. Effects of carbonate distribution inhomogeneity on the improvement level of bio-cemented sands: a DEM study. In: Barla M, Di Donna A, Sterpi D, Insana A, eds. *Challenges and Innovations in Geomechanics. IACMAG 2022. Lecture Notes in Civil Engineering, vol 288.* Cham: Springer; 2023. https://doi.org/10.1007/978-3-031-12851-$6_6$6
71. Zhao X, Shen Y, Melentijevic S, et al. The load-bearing mechanism of rock-socketed piles considering rock fragmentation. *Rock Mech Rock Eng.* 2024;54:10071–10097. https://doi.org/10.1007/s00603-024-04041-y
72. Zhu J, Zhu D. Calculation of building settlement induced by tunneling based on an equivalent beam model. *Soil Mech Found Eng.* 2022;59:411–416. https://doi.org/10.1007/s11204-022-09830-7

Latif F. Aslanov *has over 30 years of experience at the "Oil-gas" Research Project Institute of SOCAR, where he has worked in various roles, including Research Associate, Leading Research Associate, Head of the Laboratory of Marine Hydrotechnical Installations, and Head of the Technical Production Department. He is also an Associate Professor at Azerbaijan University of Architecture and Construction. His scientific and technical work has been focused on the strength, stability, durability, and operational resources of marine hydrotechnical oil and gas mining installations. Currently, his research is dedicated to evaluating the exploitation of resources of existing marine hydrotechnical structures. Prof.Dr. Aslanov has conducted numerous experimental investigations on hydrotechnical objects and large-scale models. His research on the load-bearing capacity of long-length driven piles, as well as combined drilled and cemented piles, and the stress–strain state of platform structures under static*

and dynamic loading, has made a significant contribution to the development of several normative documents, which are now widely applied.
https://orcid.org/0000-0003-1546-5436

Ulvi L. Aslanli *is a dedicated educator, senior structural engineer, and researcher with over 8 years of academic and industry experience in construction engineering. He currently serves as a lecturer in the Department of Foundations and Underground Structures at Azerbaijan Structural and Architectural University, where he teaches courses in geotechnical engineering, soil mechanics, research methods in construction, structural software, and foundation engineering practices. Additionally, he works as a senior structural engineer in the Construction Department at the State Oil Company of Azerbaijan Republic (SOCAR), where he is responsible for designing and ensuring the stability of civil and industrial structures. Ulvi holds a Master's degree in Construction Engineering and Management and is actively pursuing a Ph.D. focused on the stress–strain state of marine hydraulic structures. He has authored several peer-reviewed papers published in Web of Science and Scopus journals. Ulvi also collaborates with industry professionals to bridge the gap between theory and practice.*
https://orcid.org/0009-0001-1504-5258

An International Journal of Optimization and Control: Theories & Applications
(https://accscience.com/journal/ijocta)